NRC Publications Archive
Archives des publications du CNRC

Evaluating the flow stress of aerospace alloys for tube hydroforming process by free expansion testing
Saboori, M.; Champliaud, H.; Gholipour, J.; Gakwaya, A.; Savoie, J.; Wanjara, P.

National Research Council Canada   Conseil national de recherches Canada

Canada

ORIGINAL ARTICLE

Evaluating the flow stress of aerospace alloys for tube hydroforming process by free expansion testing

M. Saboori · H. Champliaud · J. Gholipour ·
A. Gakwaya · J. Savoie · P. Wanjara

Abstract In order to obtain accurate tube hydroforming (THF) simulation results, one of the important inputs in the finite element model (FEM) of the process is the mechanical response of the material during THF. Generally, the mechanical response is defined by the stress–strain behavior that can be determined from tensile testing of the specimens extracted either from the sheet used for roll forming of the tubes or directly from the tubes. More recently, free expansion testing has been used to characterize the mechanical response of the material for hydroforming applications. The free expansion test can emulate process conditions similar to those found during THF, and as such, can be used to obtain reliable and accurate information on the mechanical response/properties of the tubular material. The aim of this research is to present an approach for evaluating the stress–strain behavior of different materials using a 3D deformation measurement system in conjunction with an analytical model. Here, to characterize the mechanical response of the materials, free expansion and tensile testing were used for austenitic stainless steel types 321 (SS 321) and 304L (SS 304L), INCONEL® alloy 718 (IN 718), and aluminum alloy 6061 in the annealed "0" temper condition (AA 6061-0). The mechanical response of each material, measured through free expansion testing of tubular forms, was compared to the respective stress–strain behavior determined from the uniaxial tensile test using ASTM E8 geometry specimens extracted from the tubes. For each material studied in this work, the two flow stress behaviors were distinct, indicating that the test method can have a noticeable effect on the mechanical response. Finite element analysis (FEA) of the free expansion of each material was also utilized to simulate the THF process with the flow stress curves obtained experimentally; the predicted expansion and burst pressure results were close to the experimental data indicating that the approach developed and described in this work has merit for characterizing the mechanical response of aerospace alloys for hydroforming applications.

M. Saboori (✉) · H. Champliaud
École de technologie supérieure, Montréal, H3C 1 K3, Canada
e-mail: mehdi.saboori@nrc.gc.ca

H. Champliaud
e-mail: henri.champliaud@etsmtl.ca

M. Saboori · J. Gholipour · P. Wanjara
National Research Council of Canada, Aerospace,
Montréal H3T 2B2, Canada

J. Gholipour
e-mail: javad.gholipourbaradari@cnrc-nrc.gc.ca

P. Wanjara
e-mail: priti.wanjara@cnrc-nrc.gc.ca

A. Gakwaya
Laval University, Québec G1V 0A6, Canada
e-mail: augustin.gakwaya@gmc.ulaval.ca

J. Savoie
Pratt & Whitney Canada, Longueuil J4G 1A1, Canada
e-mail: jean.savoie@pwc.ca

1 Introduction

Over the last decade, tube hydroforming (THF) has become a popular technology in the automotive industry due to its capacity to manufacturing complex shapes with fewer steps than traditional stamping and welding processes. However, the application of the THF process in the aerospace sector is comparatively recent with many challenges due to the high strength and/or limited formability of aerospace materials. Compared to the other forming processes, hydroforming has many advantages, such as weight reduction through more efficient section design and manufacturing, improved structural strength, tighter manufacturing tolerances, and lower tooling cost, mainly due to fewer die components, as described by Hartl [1] for tubular products and Lang et al. [2] for both tube and sheet metal

forms. The success/failure of the THF process largely depends on many factors; Ahmed and Hashmi [3] considered the importance of the mechanical properties of the material, while Vollertsen and Plancak [4] deliberated the tool geometry and friction condition. Koç and Altan [5] examined the effect of loading path on wrinkling, bulking, and bursting during the THF process of a T-shape geometry. Later, Yang and Zhang [6] studied these effects on the free expansion process. Among the abovementioned factors, the mechanical properties (yield strength, ultimate tensile strength, and elongation) and flow characteristics of the material play a critical role in the process design for THF. In general, the material parameters and mechanical properties for FEM applications are determined by different methods such as tensile testing and/or free expansion/bulge testing. Conventionally, tensile test data have been determined from flat sheet products (i.e., materials used to manufacture the tube by roll forming, welding, and sizing) to determine the properties of the tubular forms. However, the tube manufacturing process changes the mechanical response/properties of the material from that in the initial sheet condition; for instance, Koç et al. [7] reported a difference in the flow behavior of tubular products from that of the blank sheet and Sokolowski et al. [8] confirmed this difference by performing interrupted free expansion and tensile tests for SS 304. This discrepancy in the mechanical response may be even more prominent for seamless tubes that are manufactured from billet forms that undergo substantial changes in the microstructure and, thus, the mechanical response.

In order to perform the pertinent numerical simulations of the THF process, designers need more realistic and/or accurate information on the mechanical properties of the tube. In this regard, tensile testing of the specimens extracted from the tube material as well as free expansion testing of the tube was performed by different researchers in order to determine the mechanical properties for simulating the THF process. Song et al. [9] calculated analytically the flow stress of tubular material using the free expansion process with end feeding and considered the effect of friction. More recently, Song et al. [10] evaluated the flow stress characteristics of a steel with 0.09 % carbon and 0.52 % manganese using tensile samples extracted from sheet and tube geometries. Hwang and Wang [11] evaluated the stress–strain characteristics of annealed C26800 zinc copper tubes and AISI 1215 carbon steel tubes by the free expansion process and considered their anisotropic properties. Later, Saboori et al. [12] studied the effect of different material models on predicting the expansion behavior of SS 321 during the free expansion process. Several analytical methods have been proposed to improve the accuracy of the flow stress curves for FEA of the THF process. For instance, Fuchizawa and Narazaki [13] developed an analytical model in which the profile at the free expansion region was assumed to be a circular arc and its radius of curvature was determined experimentally. Koç et al. [7] proposed a combination of an online and offline measurement procedure to determine the necessary parameters (longitudinal and circumferential radius of curvature, as well as expansion and thickness at the maximum bulge height) to calculate the stress–strain curve. Hwang and Lin [14] assumed that the profile of the bulged zone was elliptical. More recently, Hwang et al. [15] calculated the stress–strain curve from the experimental data using online measurement of the bulge height by assuming an elliptical bulge profile and measuring the thickness by cutting the tubes at different stages of the hydroforming process. Bortot et al. [16] developed an offline analytical approach using a coordinate measuring machine to measure the bulge profile and the tube thickness at different stages of the process. Lately, Aguir et al. [17] used an artificial neural networks-genetic algorithm method to identify material parameters, and Zribi et al. [18] proposed an inverse method to calculate constitutive parameters in the free expansion process.

Presently, for THF applications, knowledge of the formability of aerospace materials is quite limited, and one of the objectives of this paper is to understand how to accurately determine the mechanical properties of some aerospace alloys, such as SS 321, SS 304L, IN 718, and AA 6061-0, utilizing both the uniaxial tensile test and the free expansion test. The tensile testing was performed using specimens extracted from the tubes instead of sheets. The generated pool of data presented in this paper provides then a valuable data base for these alloys. Specifically, to determine the stress–strain curve by the free expansion test, a novel online measurement approach was developed using a 3D automated deformation measurement system (Aramis®) to extract the coordinates of the bulge profile during the test. These coordinates were used to calculate the circumferential and longitudinal curvatures, which were then utilized to determine the effective stresses and effective strains at different stages of the THF process. It is noteworthy that with this approach, all the data is generated through a single test in contrast to the conventional methods that use multiple tests to generate the same type of data. In addition, as the curvatures are calculated with the experimental coordinates, there is no assumption (circular, elliptical, etc.) associated to the shape of the section, thus resulting in more accurate analytical results with the methodology presented in this paper. The flow stresses obtained from the free expansion tests were compared with those obtained from tensile testing of the specimens extracted from the tubes for the materials considered in this work, i.e. SS 304L, SS 321, IN 718 and AA 6061-0.

2 Characterizing the flow stress of tubular materials in the THF process

In the free expansion test, the tube is first clamped between the two halves of the die as shown in Fig. 1a. The tube ends are
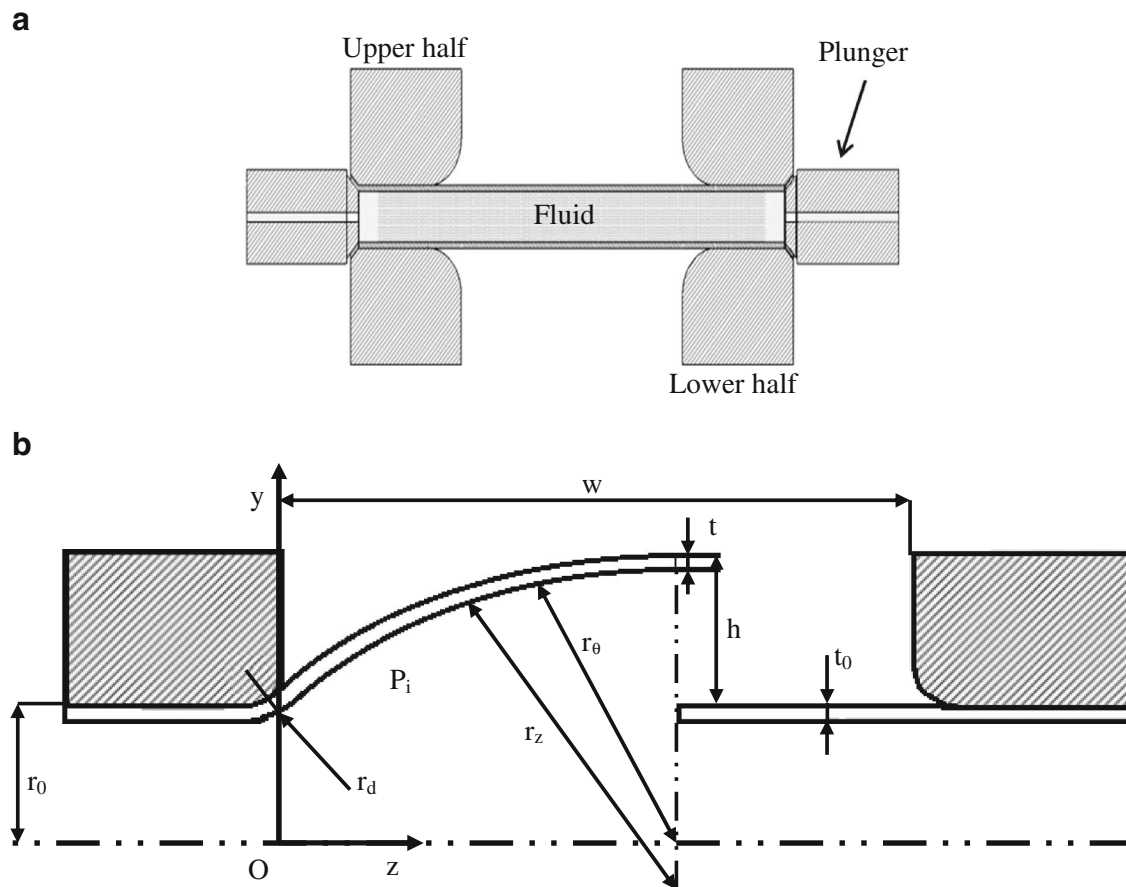
Fig. 1 Schematic diagrams of **a** the tube free expansion tool and **b** the test setup with the 3D deformation measurement system

then sealed using two plungers. Pressurized fluid is then applied into the tube through the end plungers. With increasing internal pressure, expansion (bulging) of the tube occurs and at its limit the tube bursts. It is noteworthy that the movement of the tube ends was restricted; hence, end feeding, which could push the tube material toward the expanding zone during the process, was prohibited.

Two sets of parameters, constant and variable, are involved in this process. The constant parameters comprise the length of the expansion zone (w), the die radius at the entrance of this zone (r), and the initial thickness of the tube (t_0). The variable

parameters describe the evolving bulge profile of the tube with increasing internal pressure (p) and include the bulge height (h), thickness at the maximum bulge height or pole (t), bulge circumferential radius (r_θ), and bulge longitudinal radius (r_z). In this work, these variable parameters were measured online during the hydroforming process using an Aramis® 3D
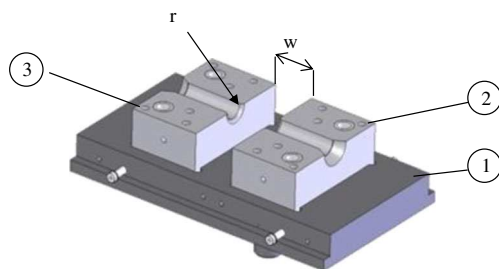

Fig. 2 CAD of the die-set: showing (*1*) the lower shoe, (*2*) the lower right cavity, and (*3*) lower left cavity
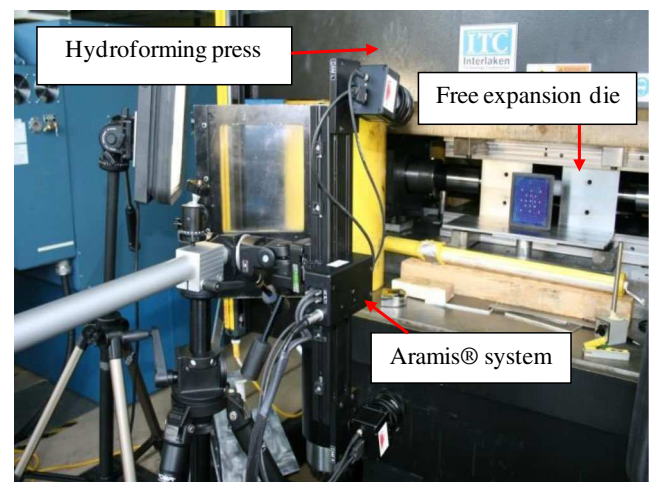

Fig. 3 Experimental setup for the free expansion tests

Table 1 Experimental conditions for the first and second set of the free expansion trials

Materials	L_0 (mm)	D_0 (mm)	w (mm)	r (mm)
SS 321 0.9 and 1.2 mm thick	228.6	50.8	101.8	7.5
IN 718 0.9 and 1.2 mm thick	228.6	50.8	101.8	7.5
SS 304L 1.6 mm thick	228.6	50.8	101.8	7.5
AA 6061-0 3 mm thick	381.0	88.9	165.0	7.5

deformation measurement system, as shown in Fig. 1b. The Aramis® system consists of two CCD cameras that can capture a predetermined number of frames per second (or steps) and uses a random dot pattern applied to the surface of the sample for measuring the deformation during the test.

In order to develop an accurate and efficient method to generate the flow stress curves for each material, a systematic and methodological approach in data acquisition from the hydroforming press and Aramis® system was established. Using the membrane theory and considering equilibrium conditions, the following equation can be written for an element of the tube at the maximum bulge height [13]:

$$\frac{\sigma_\theta}{r_\theta} + \frac{\sigma_z}{r_z} = \frac{p_i}{t_i} \qquad (1)$$

where p_i is the internal pressure and t_i is the wall thickness at stage "i." Also, σ_θ and σ_z are the circumferential and longitudinal stress components, respectively. From the force equilibrium at the maximum bulge height, the following equations have been derived [13]:

$$\sigma_z = \frac{p_i \left(r_{\theta_p} - t_p\right)^2}{2t\left(r_{\theta_p} - \frac{t_p}{2}\right)} \qquad (2)$$

$$\sigma_\theta = \frac{p_i \left(r_{\theta_p} - \frac{t_p}{2}\right)}{t_p} \times \left\{\left[1 - \frac{t_p}{2\left(r_{\theta_p} - \frac{t_p}{2}\right)}\right]\left[1 - \frac{t_p}{2\left(r_{\theta_p} - \frac{t_p}{2}\right)}\right] - \frac{\left(r_{\theta_p} - t_p\right)^2}{2\left(r_z - \frac{t_p}{2}\right)\left(r_{\theta_p} - \frac{t_p}{2}\right)}\right\} \qquad (3)$$

Fig. 4 Location of the tensile specimens extracted from seam welded SS 304L
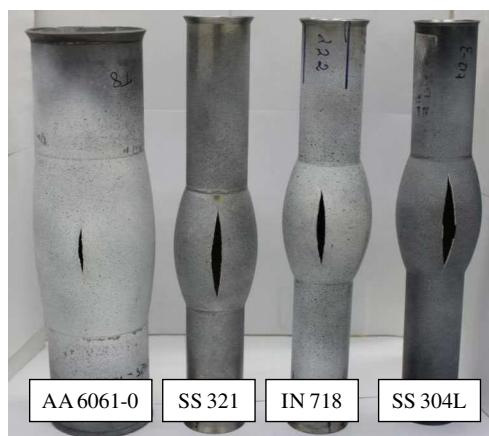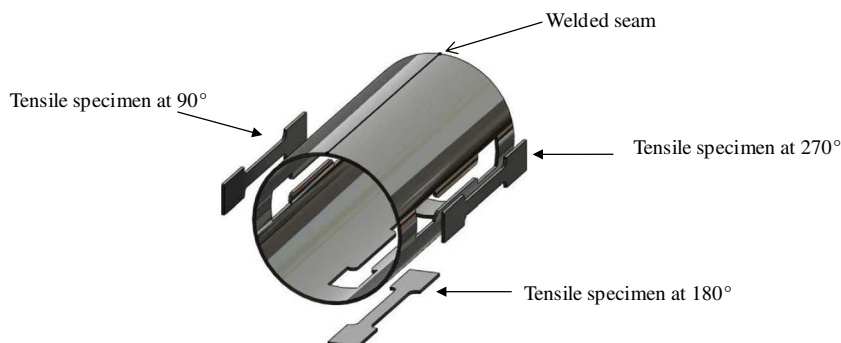
Fig. 5 AA 6061-0, SS 321, IN 718, and SS 304L tubes after free expansion testing

where r_{θ_p} is the maximum circumferential radius of curvature and t_p is the wall thickness at the maximum bulge height (i.e., at the maximum pressure).

In the free expansion process, the tube is sufficiently thin so that a plane stress state ($\sigma_t \cong 0$) can be assumed. According to Hill's yield criterion and its associated isotropic hardening law [19], the effective stress ($\overline{\sigma}$) is a function of the principal stresses as follows:

$$\overline{\sigma} = \frac{1}{2(1+R)}[(1+2R)(\sigma_\theta - \sigma_z)^m + (\sigma_\theta + \sigma_z)^m]^{\frac{1}{m}} \qquad (4)$$

Where σ_θ and σ_z are the principal stresses in the circumferential and longitudinal directions, respectively, R refers to the anisotropic parameter, and m refers to the stress exponent. The value of m is determined by the degree of anisotropy of the material and must be greater than 1 to ensure convexity of the yield surface. For different R values, the loci are ellipses when $m=2$. In the case of $R=1$, the Hill yield function transfers to the von Mises constitutive equation. The effective strain by Hill can then be calculated as a function of the principal strains as follows:

$$\overline{\varepsilon} = \frac{1}{2}[2(1+R)]^{\frac{1}{m}}\left[(\varepsilon_\theta + \varepsilon_t)^{\frac{m}{m-1}} + (1+2R)^{\frac{-1}{m-1}}(\varepsilon_\theta + \varepsilon_t)^{\frac{m}{m-1}}\right]^{\frac{m-1}{m}} \qquad (5)$$

Fig. 6 Flow chart for determining the flow curves
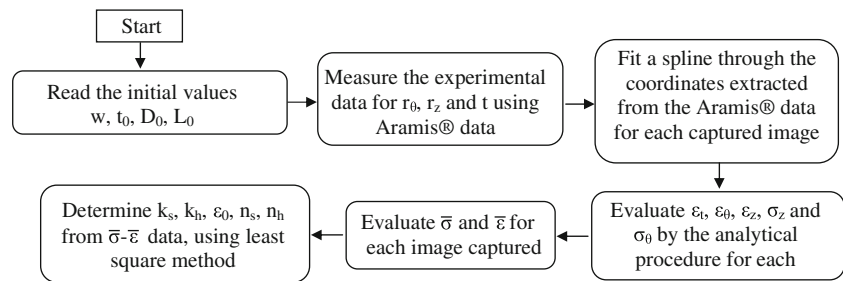
Where ε_θ and ε_t are the strains in the circumferential and thickness directions, respectively. The circumferential strain and longitudinal strain (ε_z) can be extracted from the Aramis® system so that the principal strain in the thickness direction at the maximum bulge height can be obtained through the volume constancy assumption:

$$\varepsilon_t = -(\varepsilon_\theta + \varepsilon_z) \tag{6}$$

By studying the influence of different hardening laws, it was found that the Swift hardening law (Eq. 7) can be fitted best to the experimental data for austenitic stainless steels [12, 20] for IN 718 [21] and for SS 304 [7], while for aluminum alloys, the Hollomon hardening law (Eq. 8) was reported to give the best fit [22]:

$$\overline{\sigma} = k_s \left(\varepsilon_0 + \overline{\varepsilon}_p\right)^{n_s} \tag{7}$$

$$\overline{\sigma} = k_h \left(\overline{\varepsilon}_p\right)^{n_h} \tag{8}$$

In the above equations, ε_0 is the initial plastic strain, $\overline{\varepsilon}_p$ is the effective plastic strain, k is the strength coefficient, and n is the strain hardening exponent of the material (s and h indexes correspond to Swift and Hollomon law, respectively). In Eqs. 7 and 8, to determine the flow stress curves, continuous and accurate measurements of the thickness (t), the maximum circumferential radius ($r_{\theta p}$), and the bulge curvature or longitudinal radius (r_z) are required.

In this study, to eliminate any assumption related to the bulge geometry, an Aramis® system was used to collect the data on the bulge curvature, tube thickness, bulge height, and the three principal strains at every stage of the free expansion test. To generate the bulge profile, several coordinates (z_i, y_i) were extracted along the tube length at the bulge zone from the Aramis® system, and the profile was generated by fitting a piecewise polynomial (a spline). A mathematical function of $y = f(z)$ was considered to define the bulge profile at different levels of internal pressure. This function can be written as:

$$y = az^3 + bz^2 + cz + d \tag{9}$$

where a, b, c, and d are the profile constants that must be determined during the test at each step. After taking the first and second derivatives of this function, the curvature (κ) and the value of r_z at the maximum bulge height can be determined as follows:

$$\kappa = \frac{d^2y / dz^2}{\left[1 + \left(dy/dz\right)^2\right]^{\frac{3}{2}}} \tag{10}$$

$$r_z = \left[\frac{1}{\kappa}\right]_{z = w/2} \tag{11}$$

By determining the values of the effective stress and effective strain at each Aramis® step, the biaxial flow stress curve of the tube material can be generated. At this stage, a curve fitting algorithm based on the least squares method can be used to find the constants in the different work hardening equations, such as the k and n values in Eqs. 7 and 8.

When compared to the current state-of-the-art, the innovative contribution of the methodology developed in this study is the elimination of geometric assumptions for the bulge profile (e.g., circular or elliptical), which then leads to a more reliable and accurate determination of the flow stress curves for FEA of the THF process. In addition, the continuous or online measurement capability with the Aramis® system (i.e., no interruptions for measuring the profile and/or sectioning the tubes to measure the thickness) considerably minimizes the required experimentation effort and, thus, the costs related to the tube materials, labor, and facility operation.

3 Experimental procedure

3.1 Free expansion tests

In the present study, two sets of dies, for different tube diameters, were used. Figure 2 illustrates the 3D CAD model of one of the dies used for the free expansion tests. Figure 3 shows the setup used for THF trials, which involved the use of
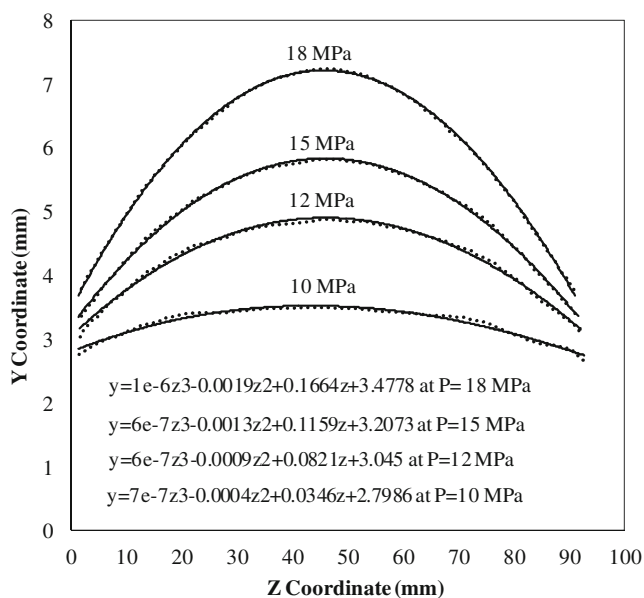
Fig. 7 Tube profile coordinates and third order spline fitted at different pressures during the free expansion process

a 1,000 ton fully instrumented hydroforming press capable of applying 400 MPa of internal pressure that was equipped with the Aramis® system and the two die sets. During the process, the ends of the tubes were maintained fixed in place and sealed using two end plungers. The experimental conditions for the two sets of free expansion experiments are given in Table 1. It is noteworthy that the first set of experiments was conducted on SS 321, IN 718, and SS 304L, while the second was performed only for AA 6061-0. To ensure the consistency of the data, each condition was repeated at least two times.

3.2 Tensile tests

Tensile specimens having a standard geometry of 50 mm in gauge length and 12.7 mm in width were machined in accordance to ASTM E8/E8M-11 [23] from the tubular material used for the free expansion tests. Specifically, the specimens were cut longitudinally from each tube, as shown in Fig. 4. With the exception of the SS 304L tubes that were seam welded, the tubes for SS 316L, IN 718, and AA 6061-0 were seamless. For the welded SS 304L tube, the specimens were extracted from three positions relative to the seamed joint (i.e., 90°, 180°, and 270° considering the weld seam being at 0°), as shown in Fig. 4. In contrast for the seamless tubes, tensile specimens were extracted from the tube at 90° intervals (i.e., 0°, 90°, 180°, and 270°). It is noteworthy that the deformation direction during hydroforming is biaxial, and the extraction of these tensile specimens from the tubes allows the measurement of the mechanical response of the material only along the longitudinal direction. All the tensile specimens were tested at room temperature and a constant crosshead rate of 2 mm/min using a 250 KN MTS testing frame equipped with a laser

video extensometer and ARAMIS® system. At least three tensile specimens for each tube material were tested to ensure test data reproducibility. The effective true stress–true strain curves were obtained by averaging the tensile test data for each tubular material.

4 Results and discussion

As mentioned previously, the free expansion tests were performed without end feeding up to the rupture/burst of the tube for each aerospace material examined in this work (i.e., SS 321, SS 304L, IN 718, and AA 6061-0) in order to determine the true stress–true strain relationships under biaxial testing conditions. Figure 5 shows examples of the free expanded tubes after bursting. A code was developed in Matlab based on the flowchart presented in Fig. 6. As indicated in this flowchart, w, t_0, D_0, R, and m were taken as the initial input, and the parameters affecting the accuracy of the calculation, h_p, t_p, r_θ, and the coordinate points (z_i, y_i), were extracted from Aramis® at different steps during the free expansion process. Then, a third order spline was fitted, as shown in Fig. 7. It should be mentioned that higher order splines (fourth and fifth orders) for fitting to the longitudinal profile were also considered, but the resulting effect on the accuracy of the fitted curve was negligible (less than 2 % at low pressures and almost zero at high pressures). For each material, the hydroforming pressure versus bulge height was then extracted from the experimental data to calculate the variables (ε_t, ε_θ, ε_z, σ_z, and σ_θ) needed to evaluate the biaxial true stress–true strain curves. Once the stress–strain response of the material was obtained, the related hardening constants for the Swift or Hollomon laws were determined numerically using the least squares method function available in the Matlab software. In this way, the associated error related to the bulge profile assumption was minimized, as the profile was determined from the real geometry of the bulge during the process.

4.1 Comparison of the tube free expansion and tensile test results

Using the methodology described above, the flow stress curves obtained under different loading conditions (biaxial from free expansion and uniaxial from tensile testing) were determined for SS 321, IN 718, SS 304L, and AA 6061-0, as presented in Fig. 8. It is noteworthy that in the case of the free expansion test data, the true stress–true strain curves plotted in Fig. 8 were determined using a spline profile (present work) and an elliptical profile (as described by Hwang et al. [15]). For AA6061-0 and SS 304L, the true stress–true strain curves determined using the free expansion test data with a spline and elliptical profiles as well as the tensile test data indicated similar flow stress behaviors; the maximum strain was greater by 0.038 for AA6061-0 and 0.054 for SS 304L under biaxial
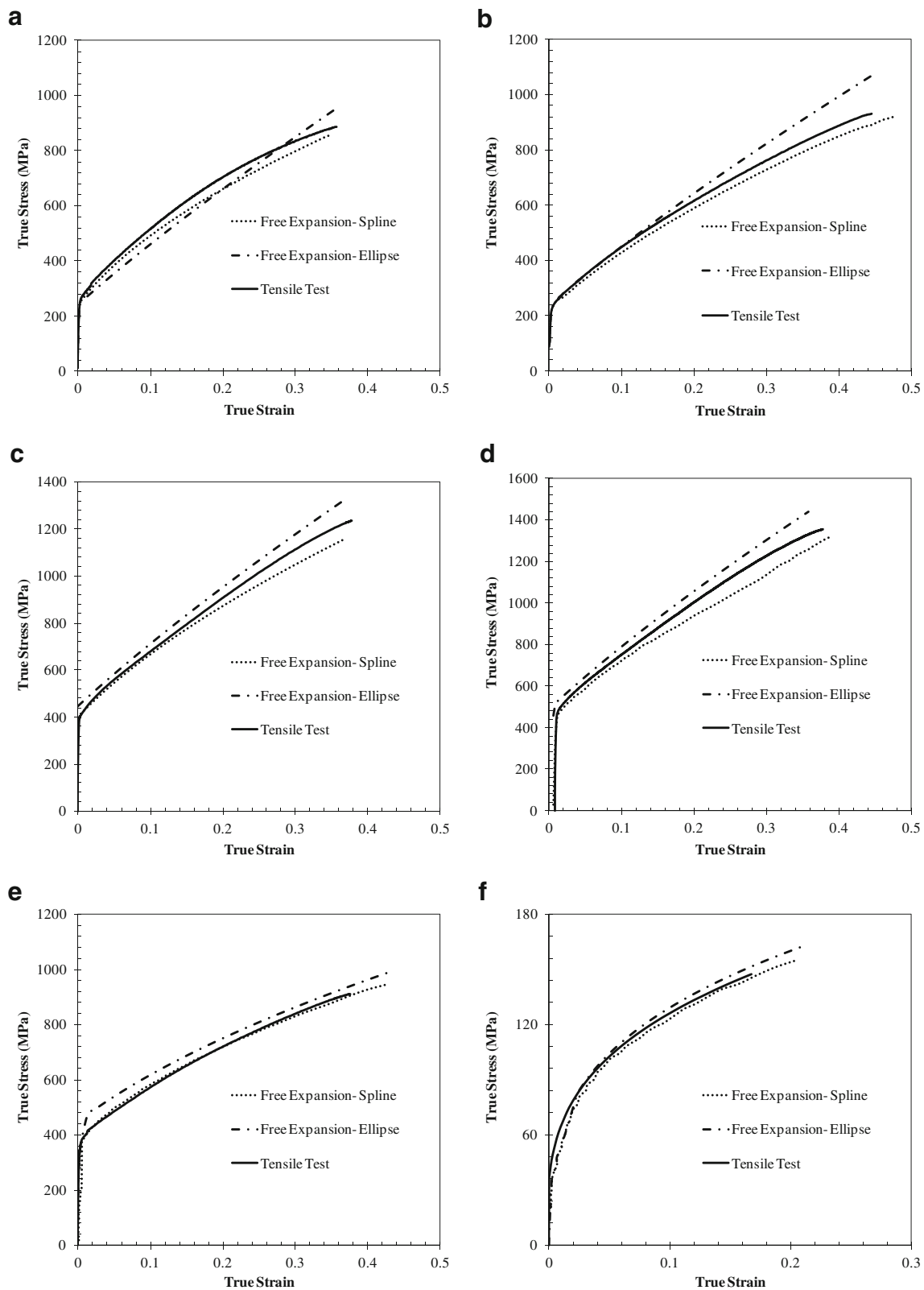
Fig. 8 Comparison of the flow stress curves for **a** SS 321, 0.9 mm thickness; **b** SS 321, 1.2 mm thickness; **c** IN 718, 0.9 mm thickness; **d** IN 718, 1.2 mm thickness; **e** SS 304L, 1.6 mm thickness; and **f** AA 6061-0, 3 mm thickness

(spline) as compared to uniaxial loading conditions. In contrast, for both IN 718 and SS 321 (0.9 and 1.2 mm thick), the

loading condition and bulge profile assumptions (spline, elliptical, etc.) have an effect on the flow stress curve.

Table 2 True stress–true strain relations based on the free expansion test results using a spline profile

Material	Thickness (mm)	Swift model $\overline{\sigma} = k_s \left(\varepsilon_0 + \overline{\varepsilon}_p \right)^{n_s}$	Hollomon model $\overline{\sigma} = k_h \left(\overline{\varepsilon}_p \right)^{n_h}$
SS 321	0.9	$\overline{\sigma} = 1,427.45 \left(0.035 + \overline{\varepsilon}_p \right)^{0.53}$	–
SS 321	1.2	$\overline{\sigma} = 1,397.81 \left(0.052 + \overline{\varepsilon}_p \right)^{0.63}$	–
IN 718	0.9	$\overline{\sigma} = 1,880.6 \left(0.072 + \overline{\varepsilon}_p \right)^{0.59}$	–
IN 718	1.2	$\overline{\sigma} = 1,980.2 \left(0.07 + \overline{\varepsilon}_p \right)^{0.62}$	–
SS 304L	1.6	$\overline{\sigma} = 1,413 \left(0.05 + \overline{\varepsilon}_p \right)^{0.47}$	–
AA 6061-0	3.0	–	$\overline{\sigma} = 267.5 \left(\overline{\varepsilon}_p \right)^{0.33}$

The relative differences in the stress–strain curves generated for the AA 6061-0 and SS 304L by means of tensile testing and free expansion testing based on the spline profile are in accordance with that expected from a fundamental perspective that the biaxial behavior is an extension of the uniaxial condition. However, for IN 718 and SS 321, the uniaxial stress–strain curve deviates from that of the biaxial and may be reasoned from a perspective of the influence of anisotropy and material microstructure (including texture) on the mechanical response. Specifically, in the case of tensile testing, the uniaxial stress–strain curve is highly dependent on the direction of sampling. Thus, depending on the relative direction of the deformation to the anisotropic property of the material, the uniaxial true stress–strain curves may then be representative or atypical of the hydroforming process. In contrast, in the case of free expansion, the average anisotropy contributes to generate the stress–strain curve, which then well represents the mechanical response of the material during the hydroforming process. Nevertheless, the material response appears to be dependent on the assumptions applied to the bulge profile (spline or elliptical), as illustrated in Fig. 8. As the online approach adopted in the present model with the spline profile calculates the evolving tube geometry during the free expansion process more accurately, it is expected that the thickness as well as the longitudinal and circumferential strains would better represent the actual conditions during THF

as compared to assuming a fixed geometry (e.g., elliptical or circular) throughout the process.

The work hardening constants of the Swift or Hollomon laws for the different materials were ascertained by the free expansion based on the spline profile and tensile tests, as shown in Tables 2 and 3, respectively. In addition, Table 4 gives the work hardening constants of the Swift or Hollomon laws for the free expansion test data obtained in the present work for the different materials but using an elliptical bulge profile. In particular, two averaged curve were generated, one from the two repetitions of the free expansion test and another from the three repetitions of the tensile test so as to calculate the respective material constants for each alloy examined in this work. Of course, for the free expansion test data, a spline or elliptical profile was included as a variant. Typically, since the loading condition in free expansion is different from that in tensile testing, the material constants obtained from the mechanical response of the material during free expansion are different from those calculated from the uniaxial tensile behavior. Interestingly, as an example, the values presented in Table 2 for 0.9 mm thick SS 321 are different from the those reported previously (k_s=1,890.85, n_s=0.84, ε_0=0.086), which were based on the assumption that the bulge profile was part of an ellipse [12]. Using the material constants in Table 2 (calculated with online measurements of the real bulge profile) and the ones presented here from previous work (with the bulge geometry assumed to be elliptical), at 0.3 strain, the effective stresses are 800 and 850 MPa, respectively. Similarly, at 0.4 strain, the effective stress values are 918 and

Table 3 True stress–true strain relations based on the tensile test results

Material	Thickness (mm)	Swift model $\overline{\sigma} = k_s \left(\varepsilon_0 + \overline{\varepsilon}_p \right)^{n_s}$	Hollomon model $\overline{\sigma} = k_h \left(\overline{\varepsilon}_p \right)^{n_h}$
SS 321[a]	0.9	$\overline{\sigma} = 1,458.29 \left(0.026 + \overline{\varepsilon}_p \right)^{0.49}$	–
SS 321[a]	1.2	$\overline{\sigma} = 1,461.54 \left(0.048 + \overline{\varepsilon}_p \right)^{0.62}$	–
IN 718[a]	0.9	$\overline{\sigma} = 2,053.36 \left(0.071 + \overline{\varepsilon}_p \right)^{0.62}$	–
IN 718[a]	1.2	$\overline{\sigma} = 2,063.85 \left(0.08 + \overline{\varepsilon}_p \right)^{0.64}$	–
SS 304L	1.6	$\overline{\sigma} = 1,350.6 \left(0.065 + \overline{\varepsilon}_p \right)^{0.47}$	–
AA 6061-0	3.0	–	$\overline{\sigma} = 239.98 \left(\overline{\varepsilon}_p \right)^{0.28}$

[a] Anderson [21]

Table 4 True stress–true strain relations based on the free expansion test results using an elliptical profile

| Material	Thickness (mm)	Swift model $\overline{\sigma} = k_s\left(\varepsilon_0 + \overline{\varepsilon}_p\right)^{n_s}$	Hollomon model $\overline{\sigma} = k_h\left(\overline{\varepsilon}_p\right)^{n_h}$
SS 321[a]	0.9	$\overline{\sigma} = 1,890.85\left(0.086 + \overline{\varepsilon}_p\right)^{0.84}$	–
SS 321	1.2	$\overline{\sigma} = 1,800.6\left(0.081 + \overline{\varepsilon}_p\right)^{0.81}$	–
IN 718	0.9	$\overline{\sigma} = 2,320.22\left(0.124 + \overline{\varepsilon}_p\right)^{0.79}$	–
IN 718	1.2	$\overline{\sigma} = 2,357.4\left(0.114 + \overline{\varepsilon}_p\right)^{0.77}$	–
SS 304L	1.6	$\overline{\sigma} = 1,399.84\left(0.11 + \overline{\varepsilon}_p\right)^{0.5}$	–
AA 6061-0	3.0	–	$\overline{\sigma} = 263.9\left(\overline{\varepsilon}_p\right)^{0.31}$

[a] Saboori et al. [12]

1,031 MPa, respectively. Hence, between the two methods, at an effective strain of 0.3 and 0.4, the difference in the effective stress is 6 and 12 %, respectively, and alludes to the impact of the bulge geometry on the mechanical response of the material.

4.2 Numerical validation

With the objective of verifying the accuracy of the proposed approach for obtaining the true stress–true strain curve of each material, results from the FE analysis of the free expansion test were compared to the experimental data. Specifically, a FE model of the free expansion test was developed and used to simulate the process for each material using the same geometrical dimensions and loading conditions applied during experimentation. Using the existing symmetry boundary conditions in the geometry, only one eighth of the die and tube materials were used in the model. Meshing was performed in ANSYS 12 software and the model was solved using LS-DYNA (V971 R6.1.2). Figure 9 shows the mesh used for the die and a tube in the FE analysis. A quadrilateral shell element with five integration points through the thickness was used for the model. The fully integrated advanced Belytschko [24] with the shell thickness change option activated was utilized as the shell element formulation. By varying the mesh size, it was found that 12,446 elements, with an aspect ratio of one for the initial (undeformed) tube, were sufficient to obtain a nearly mesh-independent solution with accurate results. The die was

modeled as a rigid body and the tube as a deformable material. In the model, a surface-to-surface contact algorithm was applied to the interface between the tube and the die with Coulomb's friction set to 0.05 in accordance with different reported values in the literature for an unlubricated condition [4, 22]. To mimic the experimental loading conditions in the FE model, the internal pressure was applied on each element of the meshed tube and increased linearly, while fixing the end nodes of the tube to emulate the no end feeding condition used during the free expansion process. The simulation results for the bulge height versus internal pressure were computed up to the maximum bulge height obtained experimentally. It is noteworthy that in the present work, the effect of anisotropy and, in the case of SS 304L only, the welded seam on the mechanical response was not considered in the FE model of the free expansion process. To this end, the effective true stress–true stain data employed in the FE model were based on the formulations given in Table 2 (spline profile) for the different alloys studied in this work. To understand the influence of different material models on the FE simulation results, the uniaxial true stress–true strain curves as formulated in Table 3 were also implemented in the free expansion model. In addition the influence of the bulge profile on the FE simulation results was considered using the formulations in Table 4 (elliptical profile).

The bulge height (h) versus internal pressure results, extracted from the simulations using the three sets of material constants (Tables 2, 3, and 4), are compared with the experimental data (obtained from Aramis® and the hydroforming press) in Fig. 10 for each alloy and thickness studied in this work. Based on the free expansion data using spline profile, the simulation results for each material is in good agreement with the experimental data, with errors less than 4 % for all the burst pressures, as demonstrated in Table 5. It is noteworthy that for 1.2 mm thick IN 718, the general behavior, calculated from the FE simulation, however, deviates somewhat from the experimental data. In the case of AA 6061-0, the bulge height behavior deviates at intermediate pressures, and this may be an effect of anisotropy in the material, the different material model (Hollomon), and/or the higher impact of any error at the

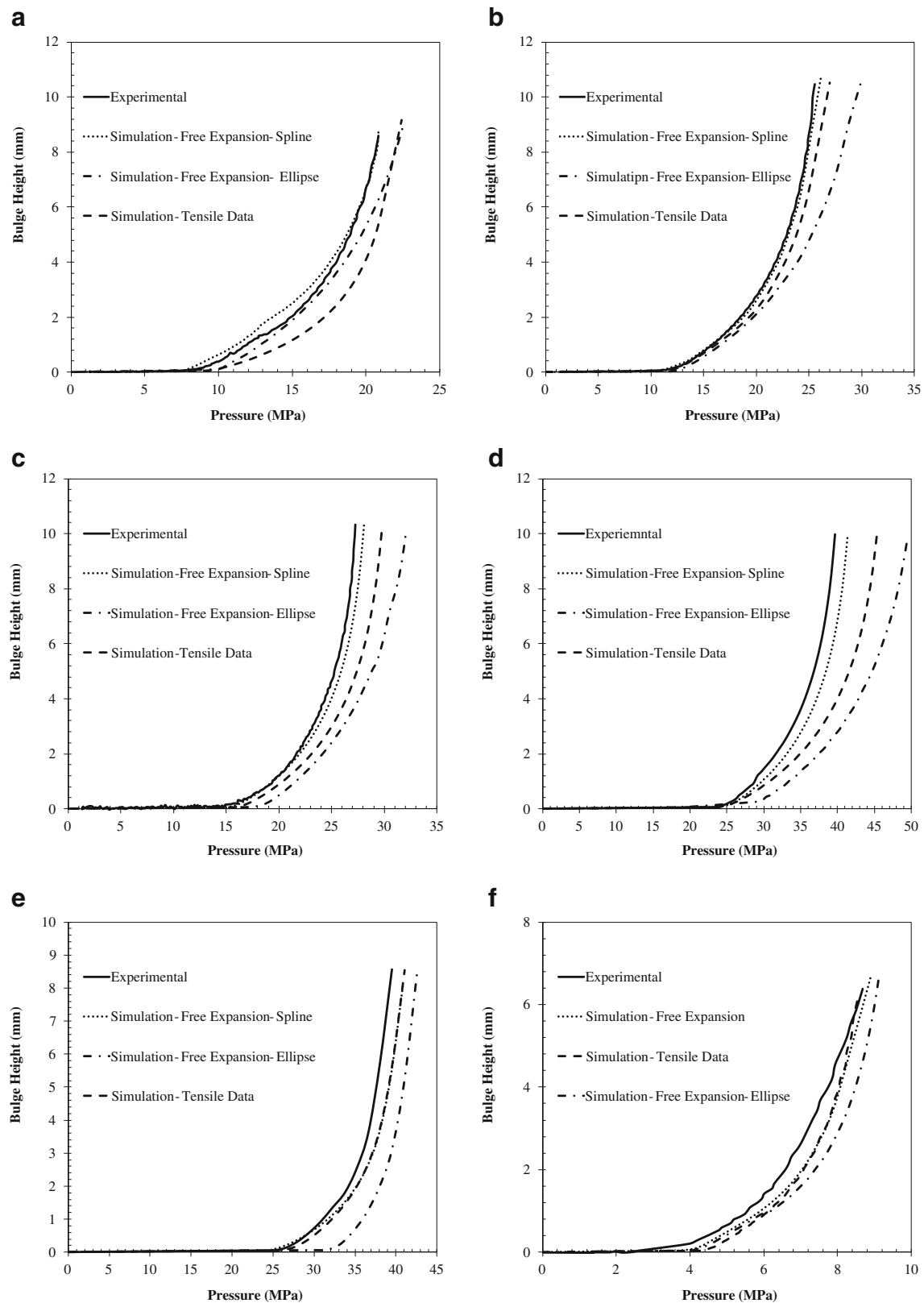
Die

Tube
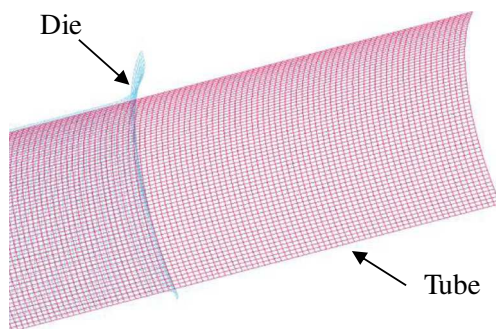
Fig. 9 Mesh used in the FEM

Fig. 10 Maximum free expansion height versus internal pressure **a** SS 321, 0.9 mm thickness; **b** SS 321, 1.2 mm thickness; **c** IN 718, 0.9 mm thickness; **d** IN 718, 1.2 mm thickness; **e** SS 304L, 1.6 mm thickness; and **f** AA 6061-0, 3 mm thickness

Table 5 Comparison of the predicted burst pressures calculated from the different material constants with the experimental data

Material	P_E (MPa)	P_{Fs} (MPa)	P_{Fe} (MPa)	P_T (MPa)	Error$_{Fs}$ (%)	Error$_{Fe}$ (%)	Error$_T$ (%)
SS 321 (0.9 mm)	20.8	20.8	27.1	27.1	0.05	30	30
SS 321 (1.2 mm)	25.6	26.2	29.9	27.1	2.5	16.9	6
IN 718 (0.9 mm)	27.2	28.1	32.1	29.8	3.2	17.8	9.5
IN 718 (1.2 mm)	39.6	40.8	48.9	45.3	2.9	23.3	14
SS 304L (1.6 mm)	39.5	40.9	42.6	41.1	3.5	7.8	4
AA 6061-0 (3 mm)	8.7	8.9	9.1	8.53	2.5	4.9	1.6

low pressures. Regardless, the use of the material constants from the free expansion test with a spline profile showed a better prediction of the burst pressure for the cases considered in this work as demonstrated in Table 5, where P_E is the experimental burst pressure, P_{Fs} and P_{Fe} are the predicted burst pressure based on free expansion data with spline and elliptical profiles, and P_T is the predicted burst pressure obtained using the tensile data.

5 Conclusions

Based on the approach proposed in this work to determine the true stress–true strain curves of different aerospace materials using the free expansion test in conjunction with the Aramis® system, the following conclusions can be drawn:

- Compared to the interrupted test methods, online measurement of the curvature and the tube thickness at the maximum bulge height along with online calculation of longitudinal and circumferential strains highly reduced the experimentation required to calculate the true stress–true strain curves from free expansion testing.
- As observed from the response of the tested materials, the true stress–true strain curve generated using a third order spline function definition for the bulge profile predicted better the material properties for the THF application.
- For each material, the simulation results of the internal pressure versus bulge height were within 4 % of the experimental data when using the true stress–true strain curve from free expansion testing concomitantly with the approach proposed in this work.

References

1. Hartl C (2005) Research and advances in fundamentals and industrial application of hydroforming. J Mater Process Technol 167:383–392
2. Lang LH, Wang ZR, Kang DC, Yuan SJ, Zhang SH, Danckert J, Nielsen KB (2004) Hydroforming highlights: sheet hydro forming and tube hydro forming. J Mater Process Technol 15:165–177
3. Ahmed M, Hashmi MSJ (1997) Estimation of machine parameters for hydraulic bulge forming of tubular components. J Mater Process Technol 64:9–23
4. Vollertsen F, Plancak P (2002) On possibilities for the determination of the coefficient of friction in hydroforming of tubes. J Mater Process Technol 125-126:412–420
5. Koç M, Altan T (2002) Prediction of forming limits and parameters in the tube hydroforming process. Int J Mach Tool Manuf 42:123–138
6. Yang B, Zhang WG (2006) Analysis and finite element simulation of the tube bulge hydroforming process. Int J Adv Manuf Technol 29:453–458. doi:10.1007/s00170-005-2548-6
7. Koç M, Aue-u-lan Y, Altan T (2001) On the characteristics of tubular materials for hydroforming: experimentation and analysis. Int J Mach Tool Manu 41:761–772
8. Sokolowski T, Gerke K, Ahmetoglu M, Altan T (2000) Evaluation of tube formability and material characteristics: hydraulic bulge testing of tubes. J Mater Process Technol 98:34–40
9. Song WJ, Kim J, Kang BS (2007) Experimental and analytical evaluation on flow stress of tubular material for tube hydroforming simulation. J Mater Process Technol 19:368–371
10. Song WJ, Heo SC, Ku TW, Kim J, Kang BS (2010) Evaluation of effect of flow stress characteristics of tubular material on forming limit in tube hydroforming process. Int J Mach Tool Manuf 50:753–764
11. Hwang YM, Wang CW (2009) Flow stress evaluation of zinc copper and carbon steel tubes by hydraulic bulge tests considering their anisotropy. J Mater Process Technol 209:4423–4428
12. Saboori M, Champliaud H, Gholipour J, Gakwaya A, Savoie J, Wanjara P (2013) Effect of material model on finite element modeling of aerospace alloys. Key Eng Mater 554-557:151-156
13. Fuchizawa S, Narazaki M (1993) Bulge test for determining stress–strain characteristics of thin tubes. Advanced Technology of Plasticity, 4th ICTP 488-493

14. Hwang YM, Lin YK (2002) Analysis and finite element simulation of the tube bulge hydroforming process. J Mater Process Technol 125–126:821-825

15. Hwang YM, Lin YK, Altan T (2007) Evaluation of tubular materials by a hydraulic bulge test. Int J Mach Tool Manuf 47:343–351

16. Bortot P, Ceretti E, Giardini C (2008) The determination of flow stress of tubular material for hydroforming application. J Mater Process Technol 203:381–388

17. Aguir H, BelHadjSalah H, Hambli R (2011) Parameter identification of an elasto-plastic behaviour using artificial neural networks–genetic algorithm method. J Mater Design 32:48–53

18. Zribi T, Khalfallah A, BelhadjSalah H (2013) Experimental characterization and inverse constitutive parameters identification of tubular materials for tube hydroforming process. J Mater Design 49:866–877

19. Hill R (1979) Theoretical plasticity of textured aggregates. Math Proc Camb Philos Soc 85:179–191

20. Saboori M, Gholipour J, Champliaud H, Gakwaya A, Savoie J, Wanjara P (2013) Development of an Inverse Method for Material Characterization, Materials Science and Technology: Symposium on Advances in Hydroelectric Turbine Manufacturing and Repair, Montreal, Canada, October 27-31

21. Anderson M, M.S.c. Thesis, (2010) Dept. of Mechanical Engineering, École de technologie Supérieure, Montreal, Canada

22. Abrantes JP, Szabo-Ponce A, Batalha GF (2005) Experimental and numerical simulation of tube hydroforming (THF). J Mater Process Technol 164–165:1140–1147

23. ASTM Committee E-28.11. (2011) Standard test method for tension testing of metallic materials. ASTM E8M-04

24. Belytschko TLI, Tsay CS (1984) Explicit algorithms for the nonlinear dynamics of shells. Comput Methods Appl Mech Eng 42:225–251